IEEE Access
Multidisciplinary | Rapid Review | Open Access Journal

Received April 3, 2019, accepted April 9, 2019, date of publication April 12, 2019, date of current version April 24, 2019.

Digital Object Identifier 10.1109/ACCESS.2019.2910882

A Novel Open Circuit Voltage Based State of Charge Estimation for Lithium-Ion Battery by Multi-Innovation Kalman Filter

ZHENG LIU[1,2], XUANJU DANG[1], AND BENQIN JING[1,2]
[1]School of Electronic and Automation, Guilin University of Electronic Technology, Guilin 541004, China
[2]School of Electronic and Automation, Guilin University of Aerospace Technology, Guilin 541004, China

Corresponding author: Xuanju Dang (xjd69@163.com)

This work was supported in part by the National Natural Science Foundation of China under Grant 61863007 and Grant 61863008, in part by the Guangxi Natural Science Foundation under Grant 2015GXNSFAA139297, Grant 2016GXNSFDA380001, and Grant 2018GXNSFAA281161, in part by the Information Science Project of Guangxi Experiment Center under Grant 20130110, and in part by the Fundamental Ability Enhancement Project for Young and Middle-aged University Teachers in Guangxi Province under Grant 2017KY0865.

ABSTRACT Accurate state of charge (SOC) estimation is a fundamental guarantee for effective development of lithium-ion power battery in electric vehicles. To improve the SOC estimation precision and robustness, a novel model-based estimation approach has been proposed. Fully giving consideration to the effect of measurement errors, the dynamic external electrical property of lithium-ion battery is approximated by a controlled auto-regressive and moving average (controlled ARMA)-based equivalent circuit model. An improved adaptive extended Kalman filter approach is developed for SOC estimation based on the multi-innovation principle. Meanwhile, the different weighting factor is added into each innovation to reduce cumulative influence of historical interference. Since the flat characteristic in OCV-SOC fitting curve enlarges the OCV-based SOC estimation error, a feedforward compensation method is introduced to reduce OCV identification error to improve OCV-based SOC estimation. The simulation and experimental results verify the validity of the proposed methodology over other estimation methods. Besides, simulated current noise is added to the condition data to prove the high precision and strong robustness of the proposed algorithm.

INDEX TERMS Lithium-ion battery, state of charge, Kalman filter, multi-innovation, OCV compensation.

I. INTRODUCTION

As growing serious problems of environmental destruction and power shortage, the discovery of new renewable power sources has increasingly become a popular research agenda recently. Due to the wide spread and development of electric vehicles (EVs), the lithium-ion battery (LIB) has widely applied for EVs because of its brilliant characteristics of long circle life, low self-discharge rate, non-memory effect and desirable safety [1], [2]. However, its features are limited due to many influence and constraint factors [3]–[5]. Hence, the battery energy management system (BMS) has been designed for its efficient performance in controlling charging and discharging. An accurate SOC estimation is a core function of BMS, which provides a fundamental principle of the LIB available capacity for maintaining a longer lasting time [6]. The accurate SOC estimation deeply influences on the time scale for charging and discharging, otherwise over-charging and over- discharging will have serious and negative impact on LIB life time and EVs driving safety [7]. Therefore, a reliable and high-precision SOC prediction method is an especially significant part in BMS to provide an effective energy control strategy [8].

SOC cannot be directly obtained through measurement by BMS. Many estimation methods have been developed to obtain SOC with measured current and voltage in recent years. In general, the SOC estimation methods can be divided into two broad categories: non-model based method and model based method.

The primary non-model based approaches are open circuit voltage (OCV) based lookup table (LUT) method [9] and Ampere - Hour counting (AH) method [10]. The LUT method

The associate editor coordinating the review of this manuscript and approving it for publication was Zhaojun Li.

2169-3536 © 2019 IEEE. Translations and content mining are permitted for academic research only.
Personal use is also permitted, but republication/redistribution requires IEEE permission.
See http://www.ieee.org/publications_standards/publications/rights/index.html for more information.

is straightforward, only by OCV-SOC fitting function. This method, however, the LUT method is not compatible with rapid SOC estimation since the LIB has to be kept in rest period for several hours until it reaches new stable state which considers the output voltage as OCV. The AH method is a convenient open-loop algorithm through accumulation of current per unit time, but it will encounter some problems like accumulative error and rounding error in real measurement, such as diffusion and drift current, etc. In addition, the non-model based method also cover artificial intelligence methods including support vector machine and artificial neural network [11]–[13]. Although those black-box methods are applied to estimate SOC with outstanding performance, but limited by many factors such as heavy training burden and long time consuming.

The model selection is a prerequisite for the model-based SOC estimation. Compared with complex electrochemical model (EM) including the internal polarization and diffusion reaction in LIB [14], the equivalent circuit model (ECM) only utilizes groups of resistance and capacitance to represent external dynamic electrical characteristic of LIB [15]. The dynamic response of LIB can be simulated by simple one-order ECM, and the model parameters are recursive identified by least squares (LS) method [16]. Although multi-order ECM can lead to better performance in representing LIB dynamic behavior than the one-order ECM, the more ECM parameters need to be identified with the increasing algorithm complexity. Therefore, the effective ECM is largely dependent on the balance between complexity and precision of corresponding algorithm.

As model-based estimation methods, the SOC can be regarded as a part of state observer. The various forms of system filtering method can be extensively accepted for SOC estimation [17]. The prevailing non-linear filtering technology is extended Kalman filter (EKF) by first order Taylor series expansion to approximate the nonlinear dynamic observation in LIB parameters identification [18]. The unscented Kalman filter (UKF) and unscented particle filter are utilized to estimate LIB SOC by the recursive unscented transformation approach without Taylor series expansion [19], and the estimation results show that the UKF has better robustness and higher precision than the EKF in SOC estimation. The cubature Kalman filter (CKF) based on radial - spherical cubature rule is adopted in SOC estimator to achieve the goal of higher precision and better stability than EKF and UKF [20], [21]. Although the UKF and CKF are superior to EKF in truncation errors and filtering divergence, the complexity of these algorithms are significantly increased. Considering the shortage of the EKF, several optimization methods are proposed. In [22], the EKF is combined with particle swarm algorithm to enhance the estimation precision of SOC. For the potential impact of inaccuracy or unknown noise in KF algorithm, a novel adaptive KF method based on the combination of Sage-Husa filter and strong tracking filter (STF) is proposed to improve the SOC estimation accuracy and robustness [23].

Since LIB OCV shows an instinct relationship with SOC, how to determine the OCV is a key problem to be firstly solved in SOC estimation. There are two major researches, such as OCV test and OCV identification. Four OCV test methods are compared in [24]. However, these offline OCV tests are cost much time, which is not suitable for real time SOC estimation. On the other hand, the OCV can be treated as sub-parameter of model parameters and identified by a variety of algorithms. In Ref. [25], the compound model parameters including OCV are identified by recursive least squares with forgetting factor (FFRLS) based on n-order RC ECM. The model components and OCV which are considered as parameters vector are identified by adaptive joint extended KF at different ambient temperatures [26]. Compared with combined parameters identification method, the OCV is firstly identified based on known parameters with incremental RLS, and then KF is added to correct identification error of OCV [27]. In view of the negative impact on OCV estimation by model uncertainty and variable parameters, the H-infinity KF with strong robustness is introduced to estimate OCV [28]. The OCV estimation capabilities at various operating conditions are compared by three estimation methods including least mean square (LMS), recursive least squares (RLS) and adaptive observer [29]. Certain fitting functions are used to describe particular relationship between OCV and SOC. In [30], the fitting function based on electrochemical principle is used to describe the relevance of OCV and SOC. In [31], four fitting functions including exponential function, polynomial function, power series model and electrochemical function are compared, and a novel sigmoid function is applied for representing the relationship between OCV and SOC. In order to reduce the fitting error, the cubic-hermite interpolation function as OCV model can be interpreted as a simplified electrochemical model [32]. Although those fitting functions can represent the nonlinear correlated behaviors of OCV and SOC, the local flat effect in fitting curve is not taken into account, consequently, just a little OCV identification error will directly cause an increase of SOC estimation error.

The main contributions of this thesis are summarized as follows: (1) An improved AEKF approach based on the multi-innovation with forgetting factors is used to develop an accurate and reliable SOC estimator, (2) Fully taken into consideration for the local flat characteristic of fitting curve, the error compensation strategy for OCV identification is used to improve the precision of OCV-based SOC estimation and (3) Compared with the wide usage of AEKF, the proposed method has the features of strong robustness and high precision.

The remainder of this paper is organized as follows. The details of LIB ECM based on controlled ARMA analysis and the ECM parameters identification by variable FFRLS (VFFRLS) method is presented in Section 2. The improved AEKF based on multi-innovation with forgetting factors and OCV compensation strategy is presented in Section 3. Section 4 compares the experimental results under the DST

and FUDS conditions. Finally, some concluding remarks are given in Section 5.

II. BATTERY MODEL AND PARAMETERS IDENTIFICATION

A. BATTERY MODEL

As a balance method between model precise and model complexity, ECMs with different orders are used extensively in the proposed battery models. In this paper, a simplified ECM including one-order RC network is utilized for representing the external electrical characteristics of LIB to make a compromise between model precision and complexity. As shown in Fig.1, the ECM includes a resistor R_0 one-order network with R_pC_p. The resistor R_0 is the ohmic resistance (the resistance $R_{0,chg}$ denotes discharge ohmic resistance, and the resistance $R_{0,chg}$ denotes charge ohmic resistance), while R_pC_p is employed to approximate the over-potential dynamics of LIB.

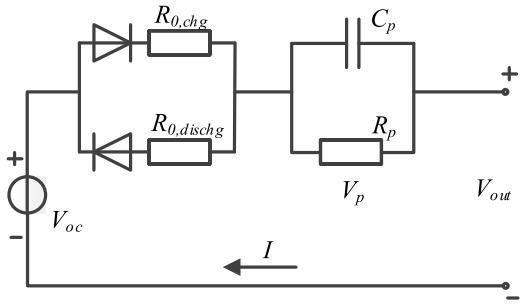

FIGURE 1. Schematic diagram of the one-order RC ECM.

According to circuit principle, one-order ECM can be expressed as:

$$\begin{cases} \dot{V}_{p,t} = -\dfrac{V_{p,t}}{R_pC_p} + \dfrac{I_t}{C_p} \\ V_{out,t} = V_{oc,t} - V_{p,t} - R_0I_t \end{cases} \tag{1}$$

where $V_{oc,t}$ describes OCV which associates with SOC, $V_{p,t}$ represents polarization voltage across R_pC_p,I_t is the charging-discharging current, and $V_{out,t}$ represents the output voltage.

SOC indicates the proportional of the remaining capacity to the rated capacity of LIB. Mathematically, a common definition of SOC can be expressed as:

$$SOC_t = SOC_{t-1} + \frac{\int_{t_0}^{t} I_t dt}{Q_N} \tag{2}$$

where I_t and SOC_t represent the current and SOC at time t, respectively. Q_N is the rated capacity.

The state equation of SOC can be described as a discrete-time form:

$$SOC_{k+1} = SOC_k + \frac{\eta I_k}{Q_N} \tag{3}$$

B. PARAMETERS IDENTIFICATION

For the one-order ECM shown in Fig.1, the identified parameters covering R_0, R_p and C_p.

The polarization voltage V_p can be eliminated from Eq. (1). The transfer function G(s) of the ECM can be drawn as:

$$G(s) = \frac{V_{out}(s) - V_{oc}(s)}{I(s)} = R_0 + \frac{R_p}{1 + R_pC_ps} \tag{4}$$

The discretization form of Eq. (4) by bilinear transformation method: $s = \frac{2}{T_s}\frac{1-z^{-1}}{1+z^{-1}}$ (z is the discretization operator) is given as:

$$G(z^{-1}) = \frac{V_{out}(z^{-1}) - V_{oc}(z^{-1})}{I(z^{-1})} = \frac{b_1 + b_2z^{-1}}{1 + a_1z^{-1}} \tag{5}$$

where

$$a_1 = \frac{(2R_pC_p - 1)}{(1 + 2R_pC_p)}, \quad b_1 = \frac{-(2R_0R_pC_p + R_0 + R_p)}{(1 + 2R_pC_p)},$$
$$b_2 = \frac{(2R_0R_pC_p - R_0 - R_p)}{(1 + 2R_pC_p)}.$$

According to the time-domain relationship between the input and the output, $G(z^{-1})$ can be rewritten in a regression form after discretization as follows:

$$V_{out,k} = a_1V_{out,k-1} + b_1I_k + b_2I_{k-1} + (1 - a_1)V_{oc,k} \tag{6}$$

Given the random noise in current sensor and voltage sensor, the random noises in $V_{out,k}$, $V_{out,k-1}$, I_k and I_{k-1} are ignored in Eq. (6). Assumed the random noises are added in $V_{out,k}$, $V_{out,k-1}$, I_k, I_{k-1}, namely:

$$\begin{cases} V_{out,k} = \overline{V}_{out,k} + c_1e_k \\ V_{out,k-1} = \overline{V}_{out,k-1} + c_1e_{k-1} \\ I_{out,k} = \overline{I}_{out,k} + c_2e_k \\ I_{out,k-1} = \overline{I}_{out,k-1} + c_2e_{k-1} \end{cases} \tag{7}$$

Substituting Eq. (7) into Eq. (6) yields the following expression.

$$\begin{aligned} V_{out,k} = a_1\overline{V}_{out,k-1} + b_1\overline{I}_k + b_2\overline{I}_{k-1} + (1 - a_1)V_{oc,k} \\ +a_1c_1e_{k-1} + b_1c_2e_k + b_2c_2e_{k-1} + c_1e_k \end{aligned} \tag{8}$$

It's clear from Eq. (8) that expression meets the requirement of controlled ARMA characteristics [11]. According to the definition of controlled ARMA, the designed ECM of LIB can be rewritten in Eq. (9):

$$A(z^{-1})y_k = B(z^{-1})x_k + C(z^{-1})e_k \tag{9}$$

where $A(z^{-1})$,$B(z^{-1})$ and $C(z^{-1})$ are the coefficients of the controlled ARMA ECM.

Combining Eqs. (7) and (8), the discrete LIB model is deduced as.

$$\begin{cases} V_{out,k} = a_1V_{out,k-1} + b_1I_k + b_2I_{k-1} \\ \qquad +(1 - a_1)V_{oc,k} + c_1e_k \\ e_k = e_{k-1} + \varepsilon_k \end{cases} \tag{10}$$

In accordance with nonlinear regression mode principle, the Eq. (10) can be rewritten as least-square form:

$$V_{out,k} = \phi_k^T\theta_k \tag{11}$$

where

$$\begin{cases} \phi_k = \begin{bmatrix} V_{out,k-1} & I_k & I_{k-1} & 1 & e_k \end{bmatrix}^T \\ \theta_k = \begin{bmatrix} a_1 & b_1 & b_2 & (1-a_1)V_{oc,k}c_1 \end{bmatrix} \end{cases} \tag{12}$$

In Eqs. (11) and (12), θ_k is the unknown parameter, ϕ_k is the known coefficient determined by measurement, $e_0 = 0$, $\hat{V}_{out,k} = \phi_k^T \hat{\theta}_{k-1}$ and $e_k = V_{out,k} - \phi_k^T \hat{\theta}_k$.

In consideration of fact that the model parameters may change with different rates [33], the VFFRLS [34], [35] algorithm is applied for model parameters identification, which allows forgetting factors to be decomposed and adjusted respectively to enhance the parameters identification stability and contribute to the improvement of SOC estimation.

III. OCV COMPENSATION BASED SOC ESTIMATION BY MI-AEKF ALGORITHM

A. REVIEW OF AEKF

In consider of a nonlinear system with Gaussian noises, the corresponding discrete state equation is as follows:

$$\begin{cases} x_k = A_k x_{k-1} + B_k u_{k-1} + w_{k-1} \\ y_k = C_k x_k + D_k u_k + v_k \end{cases} \tag{13}$$

where x_k is the system state vector at time k,A_k and B_k represents the dynamic property of state formula, C_k and D_k describe the dynamic property of observation formula,y_k is the measured value,u_k is the input variable. w_k and v_k are the Gaussian white noises, the covariance ofw_k and v_k is Q_k and R_k, respectively. Q_k and R_k can be estimated based on the principle of covariance-matching method [36]. The process of AEKF algorithm is listed as follows:

(I) Initialization:

$$\left\{\hat{x}_0,\ P_0,\ Q_0,\ R_0\right\} \tag{14}$$

(II) Prior estimation

Update the step state

$$\hat{x}_{k|k-1} = A_k \hat{x}_{k-1|k-1} + B_k u_{k-1} \tag{15}$$

Update the step error covariance

$$P_{k|k-1} = A_k P_{k-1|k-1} A_k^T + Q_{k-1} \tag{16}$$

(III) Measurement correction

Single error innovation

$$e_k = y_k - C_k \hat{x}_{k|k-1} - D_k u_k \tag{17}$$

Calculate gain matrix

$$K_k = P_{k|k-1} C_k^T (C_k P_{k|k-1} C_k^T + R_k)^{-1} \tag{18}$$

State measurement update

$$\hat{x}_{k|k} = \hat{x}_{k|k-1} + K_k e_k \tag{19}$$

Error covariance measurement update

$$P_{k|k} = (I - K_k C_k) P_{k|k-1} \tag{20}$$

(IV) Adaptive covariance-matching of Q_k and R_k

$$\begin{cases} Q_k = K_k F_k K_k^T \\ F_k = \frac{1}{M} \sum_{i=k-M+1}^{k} e_k e_k^T \\ R_k = F_k - C_k P_{k|k-1} C_k^T \end{cases} \tag{21}$$

Eqs. (14-21) compose the process of AEKF algorithm based on the principle of covariance- matching. However, the expression of R_k in Eq. (21) cannot guarantee the positive definiteness of R_k in real time. For the estimation of R_k, Eq. (22) replaces the expression of R_k in Eq. (21) to ensure the positive definiteness of R_k during the covariance updating process.

$$R_k = F_k + C_k P_{k|k-1} C_k^T \tag{22}$$

B. MULTI-INNOVATION BASED MI-AEKF

The multi-innovation identification method includes multi-step predictive information in iterative process, which was brought forward firstly by Ding *et al.* [37]. From Eq. (17) only single innovation is used as prediction error, which may result in a loss of information for posterior measurement correction. Combined the multi-innovation and EKF (MI-EKF) is beneficial for improving error correction effect in contrast with EKF with single innovation (SI-EKF) [23]. Although the computation quantity of MI-EKF will slightly increase, the cost of MI-EKF is acceptable in consideration of improvement of estimation precision.

The traditional EKF can be extended to MI-EKF by multi-innovation method. Obviously, it is the direct way that extends a single innovation e_k to be an innovation vector $E_{p,k}$.

$$E_{p,k} = \begin{bmatrix} e_k \\ e_{k-1} \\ e_{k-2} \\ \vdots \\ e_{k-p+1} \end{bmatrix} = \begin{bmatrix} y_k - C_k \hat{x}_{k|k-1} \\ y_{k-1} - C_{k-1} \hat{x}_{k-1|k-2} \\ y_{k-2} - C_{k-2} \hat{x}_{k-2|k-3} \\ \vdots \\ y_{k-p+1} - C_{k-p+1} \hat{x}_{k-p+1|k-p} \end{bmatrix} \tag{23}$$

Meanwhile, the gain K_k can be expended as gain matrix $K_{p,k}$:

$$K_{p,k} = [K_{1,k},\ K_{2,k}, \cdots K_{p,k}] \in R^{n \times p} \tag{24}$$

Consequently, the state measurement update needs to be revised as following:

$$\begin{aligned} \hat{x}_{k|k} &= \hat{x}_{k|k-1} + [K_{1,k},\ K_{2,k}, \cdots K_{p,k}] E_{p,k} \\ &= \hat{x}_{k|k-1} + \sum_{i=1}^{p} K_{i,k} e_{k-i+1} \end{aligned} \tag{25}$$

where $K_{i,k}$ is gain matrix at times k, $E_{p,k}$ is innovation matrix, p is the length of innovation, the MI-EKF can be regarded as SI-EKF when $K_{2,k} = K_{3,k} \cdots = K_{p,k} = 0$. Not only the state at time (k-1) is considered but the states at times (k-i) are taken into accounted by MI-EKF.

The procedure of MI-EKF which the past multi-states are combined into EKF to estimate the state of LIB at the current time (k) is as follow:

$$\begin{cases} \hat{x}_{k|k-1} = A_k \hat{x}_{k-1|k-1} + B_k u_{k-1} \\ P_{k|k-1} = A_k P_{k-1|k-1} A_k^T + Q_{k-1} \\ e_{k-p+1} = y_{k-p+1} - C_{k-p+1} \hat{x}_{k-p+1|k-p} - D_{k-p+1} u_{k-p+1} \\ K_k = P_{k|k-1} C_k^T (C_k P_{k|k-1} C_k^T + R_k)^{-1} \\ \hat{x}_{k|k} = \hat{x}_{k|k-1} + \sum_{i=1}^{p} K_{i,k} e_{k-i+1} \\ P_{k|k} = (I - K_k C_k) P_{k|k-1} \end{cases} \tag{26}$$

When a series of old measurement are introduced as correction term in the state measurement update, the old data may results in accumulative interference since the measurement errors are exist in output voltage and current. In addition, the influence of new measurement should be greater than that of old measurement. From the discussion of KF with fading factors [38], the adverse effect of old measurement and new measurement both are equally weighted, which may result in accumulative interference. In this case, different weighting factors are introduced into different innovations to reduce correction effect of old data. The state measurement update with multi-innovation is as follows:

$$\hat{x}_{k|k} = \hat{x}_{k|k-1} + \sum_{i=1}^{p} \lambda_i K_{i,k} e_{k-i+1} \tag{27}$$

In order to ensure maximum weight of gain at current time, the weights at different times can be defined as:

$$\lambda_1 \geq (\lambda_2 + \lambda_3 + \cdots \lambda_p) \tag{28}$$

Through adding different weighting factors into gains at different times, the comparative balance between effective correction and suppression of accumulative interference can be achieved. For the performance of MI-EKF, it is at least superior to the EKF, the different weights are as follow:

$$\begin{cases} \lambda_1 = 1 \\ \lambda_2 = \lambda_3 = \cdots \lambda_p = \dfrac{a}{p-1}, 0 \leq a \leq 1 \end{cases} \tag{29}$$

where p is the length of innovation, adjustable coefficient a is 0.5.

Although the appropriate multi-innovation coupling EKF is benefit to improve estimation precision, the more innovations are added, the better performance is not always obtained. The definitive innovation data is the key player to ensure effect of MI-AEKF because the innovation length must be constrained to a certain value.

C. OCV COMPENSATION STRATEGY

1) ANALYSIS ON LIB OCV-SOC FITTING CURVE

In generally, the relationship between SOC and OCV is considered as known information for SOC estimation and the OCV is calculated by parameters identification method. In this paper, the 8th-order polynomial fitted function is used to describe the relationship between SOC and OCV:

$$V_{oc}(k) = \sum_{i=0}^{N} b_i SOC(k)^i \tag{30}$$

where V_{oc} is the OCV, b_i is the polynomial fitting coefficient, N is the order of fitting function and N is set to 8.

The $OCV - SOC$ fitting curve of LIB based on Eq. (30) is illustrated in Fig. 2(a). It should be noted that (1) Because the LIB OCV is identified as a part of parameters based on charge/discharge current and output voltage, the precision of measurements directly impact the identification precision of OCV and (2) the mapping between OCV and SOC is sensitive to the health status and depth of discharge/charge of LIB. More particularly, there exists a local flat region in the $OCV - SOC$ fitting curve where the SOC ranges from 0.2 to 0.8. Even if the measurement error of voltage and current is relatively slight, the identification error of OCV may lead to a relatively large estimation error of SOC.

The curve of $dSOC/dOCV$ in Fig. 2(b) is the variation of SOC per mV of OCV changing in the $OCV - SOC$ fitting curve. It's worth noting that the variation of the $dSOC/dOCV$ curve obviously increases when the OCV ranges from 25.5 to 26.5V, correspondingly, the SOC ranges from 0.2 to 0.8. That is, the SOC estimation is particularly sensitivity to identified OCV in the special area by considering the intrinsic OCV variation. Thus, the SOC estimation based on the basic fitting function may imply greater risk of interference in the local flat region of $OCV - SOC$ fitting curve.

From the analysis above, the OCV error may largely decline the accuracy of SOC estimation. It's essential to make an adequate compensation for OCV especially when the SOC falls into the ranges from 0.2 to 0.8.

2) FEEDFORWARD COMPENSATION FOR OCV IDENTIFICATION BY OUTPUT VOLTAGE DEVIATION

Since the OCV that has strong correlation with $OCV - SOC$ fitting function is highly similar to the output voltage when the LIB is close to stable state, the output voltage is approximately regarded as the OCV because the output voltage can be directly measured by test system. In the same way, the residual error of output voltage is employed to approximately represent the features of deviation of OCV. Because the improvement of SOC estimation can be implemented by the deviation of OCV identification, the residual error of output voltage is used for compensating error of SOC estimation.

The residual error of output voltage cannot completely cover the features of the deviation of OCV. Therefore, a micro-correction term need be adopted for compensating error of OCV caused by residual error of output voltage. The simple correction formula is shown as Eq. (16):

$$\Delta \hat{V}_{oc}(k) = (df(soc)/dsoc) \left(V_{out}(t) - \hat{V}_{out}(t) \right) \tag{31}$$

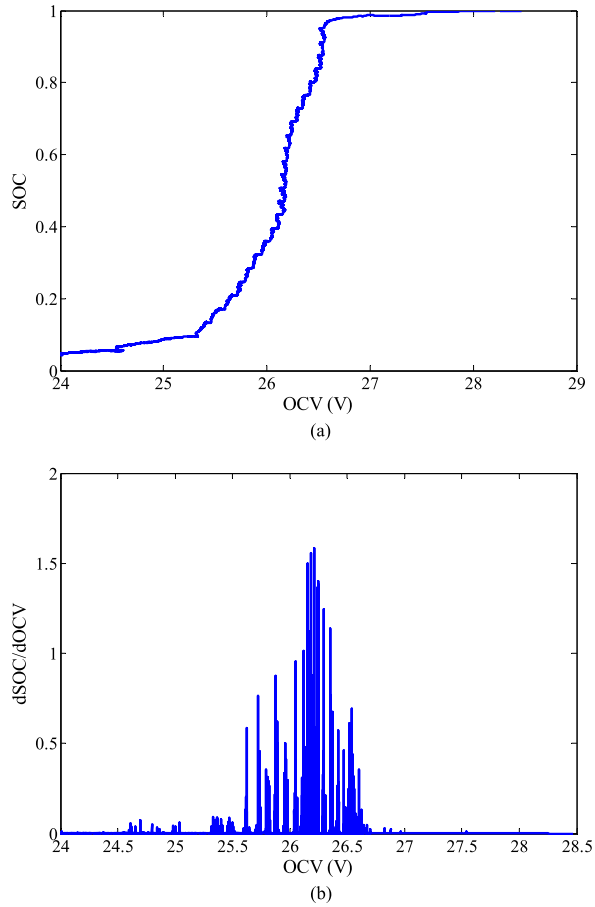

FIGURE 2. (a) OCV-SOC curve; (b) SOC variation per OCV.

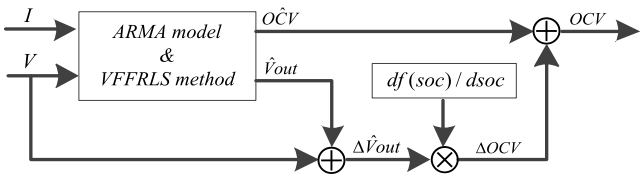

FIGURE 3. The block diagram of OCV compensation algorithm.

where $\Delta\hat{V}_{oc}$ is used as compensation module at time k, $(df(soc)/dsoc)$ is the micro-correction term for residual error of output voltage.

The micro-correction term $(df(soc)/dsoc)$ is determined by the gradient of LIB $OCV-SOC$ fitting curve as illustrated in Fig. 2(b). The faster the SOC changes, the OCV error is greater when the value scope for OCV ranges from 25.5 to 26.5V (SOC ranges from 0.2 to 0.8). To make up the obvious disadvantage in that sensitivity region, the appropriate correction term must be adaptively changed along with the change rate of SOC. The stronger SOC gradient varies, the greater correction term should configure. Hence, the OCV feedback compensation term is only applied in defined area which belongs to local flat area (SOC ranges from 0.2 to 0.8).

The block diagram of feedforward compensation for OCV identification by output voltage deviation is shown in Fig. 3.

As illustrated in Fig. 3, the premise of compensation method is that the identification of OCV and output voltage can be obtained by the combination of ARMA model and VFFRLS method. The difference of output voltage between estimate and measurement is used as residual error of output voltage $(\Delta\hat{V}_{out})$. The residual error $(\Delta\hat{V}_{out})$ and micro-correction term $(df(soc)/dsoc)$ are utilized to get corresponding compensation term (ΔOCV) to correct the OCV identification by the feedforward method. To some degree, the feedforward compensation method not only balances out the OCV identification error due to the local flat effect of $OCV-SOC$ fitting curve, but also improves the estimation precision of SOC.

D. SOC ESTIMATOR BY COMBINING MI-AEKF AND OCV COMPENSATION

According to the above discussion, the VFFRLS algorithm and one-order ECM with ARMA model analysis can be used for ECM parameters identification. Meanwhile the combination of MI-AEKF and OCV compensation is applied for SOC estimation. Based on the characteristic of one-order ECM, polarization voltage V_p and SOC are chosen as the state, corresponding to the discrete equation of state and measurement is shown as:

$$\begin{cases} V_{out,k} = V_{oc,k} - V_{p,k} - R_{0,k} i_k \\ V_{p,k} = e^{-\frac{1}{R_{p,k-1}C_{p,k-1}}} V_{p,k-1} \\ \qquad +(1 - e^{-\frac{1}{R_{p,k-1}C_{p,k-1}}}) R_{p,k-1} i_{k-1} \\ SOC_k = SOC_{k-1} - \dfrac{\eta T i_{k-1}}{C_{cap}} \end{cases} \tag{32}$$

where $V_{out,k}$, $V_{oc,k}$, $V_{p,k}$ are the OCV, output voltage and polarization voltage at the sample time k, respectively, and the C_{cap} is the capacity which is considered as a known state.

From the discrete ECM expression shown in Eq. (32), the state-space equation of SOC can be described in Eq. (33).

$$\begin{cases} x_k = f(x_{k-1}, u_{k-1}) + w_{k-1} = A_{k-1} x_{k-1} \\ \qquad +B_{k-1} i_{k-1} + w_{k-1} \\ y_k = h(x_k, u_k) + v_k = C_k x_k + D_k i_k + v_k \end{cases} \tag{33}$$

where

$$A_{k-1} = \frac{df(x_{k-1}, \hat{\varphi}_{k|k-1}, u_{k-1})}{dx_{k-1}}\Big|_{\hat{x}_{k|k-1}} = \begin{bmatrix} 1 & 0 \\ 0 & e^{\frac{-1}{R_{p,k-1}C_{p,k-1}}} \end{bmatrix},$$

$$B_{k-1} = \begin{bmatrix} -\dfrac{\eta_i \Delta t}{C_{cap}} & (1 - e^{\frac{-1}{R_{p,k-1}C_{p,k-1}}}) R_{p,k-1} \end{bmatrix}^T,$$

$$D_k = \begin{bmatrix} -R_{0,k} \end{bmatrix}, \quad C_k = \frac{dh(x_k, \hat{\varphi}_{k|k-1}, u_k)}{dx_k}\Big|_{\hat{x}_{k|k-1}}$$

$$= \begin{bmatrix} \frac{\partial V_{oc,k}(SOC_k, C_{cap,k})}{\partial SOC_k}\Big|_{SOC_k = SOC_{k|k-1}} & -1 \end{bmatrix}^T, x_k$$

$$= \begin{bmatrix} SOC_k & V_{p,k} \end{bmatrix}^T, y_k = \begin{bmatrix} V_{out,k} \end{bmatrix},$$

the symbol w_{k-1} represents the state noise of the x_k, the symbol v_k is the measurement noise.

With the equations of state and observation above, the LIB SOC is estimated by the improved AEKF. The process of the MI-AEKF for the SOC estimation can be

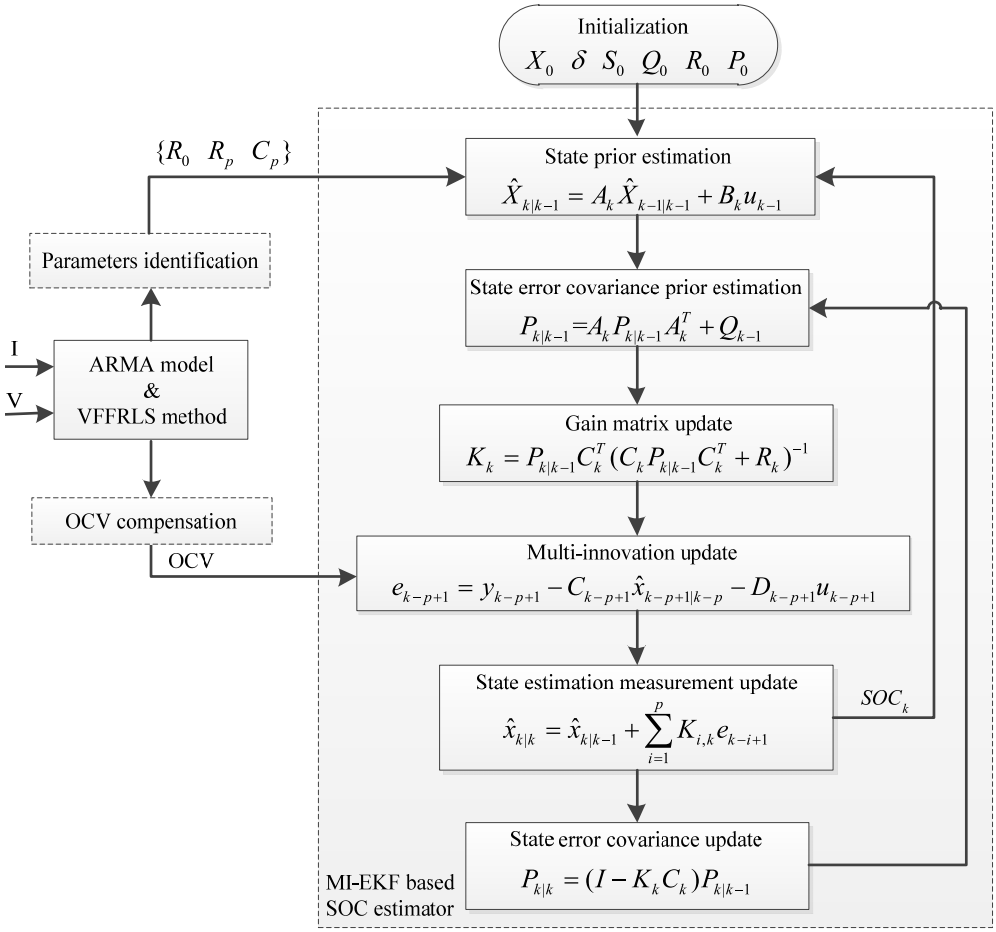

FIGURE 4. Schematic diagram of SOC estimator.

seen in Eqs. (26-29), and the feedfoward compensation for OCV identification by output voltage deviation is given in Eqs. (30-31). The whole iterative process is illustrated in Fig. (4).

IV. EXPERIMENTS RESULTS AND ANALYSIS

A high precise battery test platform is established to check and validate the proposed parameters identification and SOC estimation. The 20Ah/24V lithium-ion phosphate battery is selected as the test objects based on a high precise battery test platform, in which consists of a programmable temperature chamber, a connected computer and a power battery test system (Arbin EVTS) with current (0 to 300A) and voltage (0 to 400V), while the voltage and current measurement errors limits are both within 0.1%. The computer connecting with Arbin EVTS is used to collect and store experimental data such as charge/discharge current, output voltage at a time interval of 1s. The LIB is fully charged by constant-current-constant-voltage (CCCV) method, and then it is left to rest for two hours before being discharged. The data of DST and FUDS cycles is employed to evaluate the improved method for SOC estimation. The load current and output voltage of two conditions are shown in Figs. 5-6, where Fig. 5 (b) and Fig. 6 (b) are expanded current configuration for DST cycle and expanded current configuration for FUDS cycle, respectively. With the data flows of collected discharge current and output voltage, the VFFRLS algorithm is used to identify the ECM parameters. The identified ECM parameters versus time is shown in Fig. 5 (d) and Fig. 6 (d), the identification values of ECM parameters are able to converge to stable values rapidly from the unreliable initial value. The reference SOC should be pre-determined accurately as assessment criteria to compare with SOC estimation. The coulomb counting (CC) method with high reliability through Arbin EVTS is used to calculate the reference SOC under certain condition when initial SOC is considered to be a known value. In addition, the statistical index, such as maximum absolute error (MAE) and average absolute error (AAE), represents quantization performance of estimation algorithms.

A. PRE-DETERMINATION OF MULTI-INNOVATION LENGTH

As a matter of fact, the multi-innovation length affects the MI-AEKF algorithm performance. If the multi-innovation length is 1, the proposed MI-AEKF algorithm degrades into

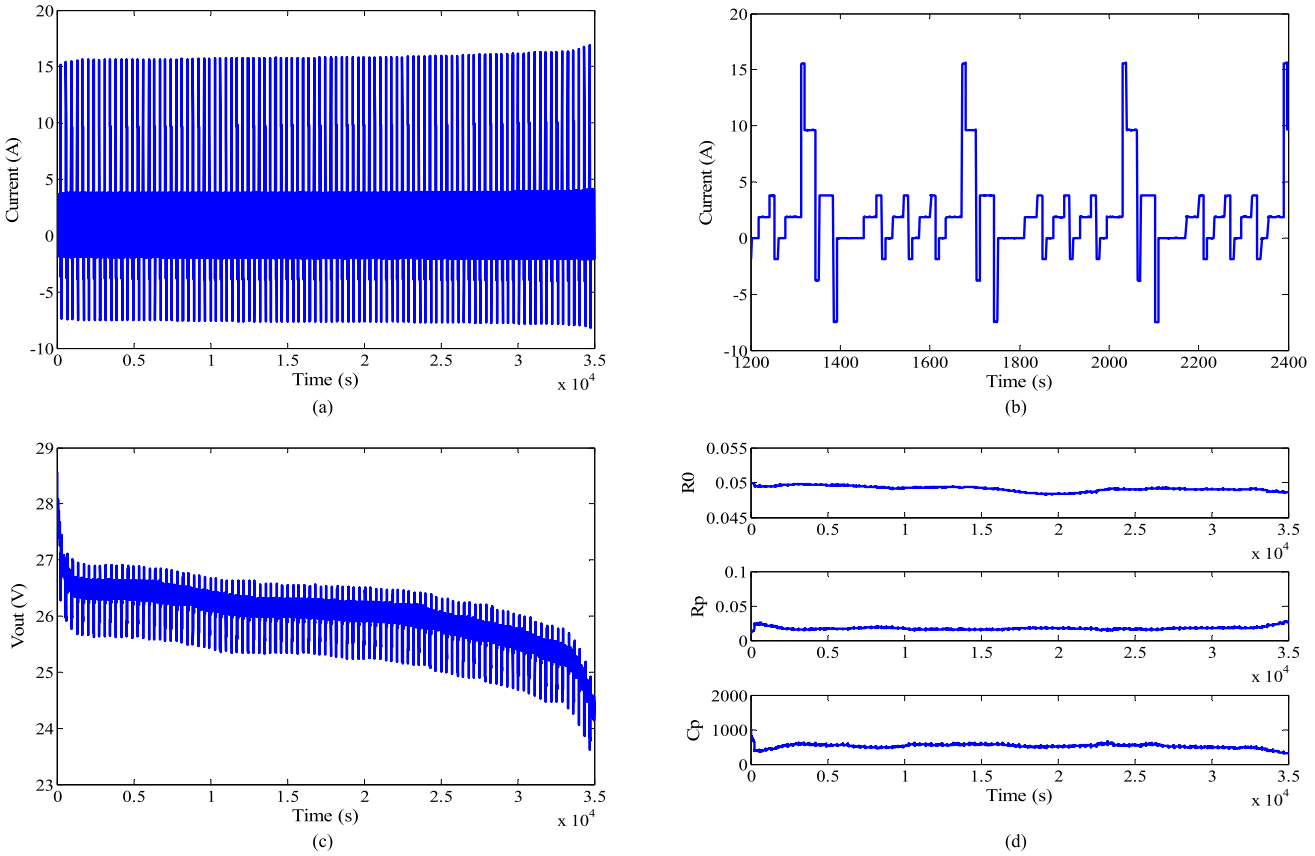

FIGURE 5. (a) Current under DST cycle; (b) enlarged current under DST cycle; (c) output voltage under DST cycle; (d) Identification value of R0, Rp, Cp under DST cycle.

general AEKF algorithm. The multi-innovation length is the crucial factor need to be determined for keeping effectiveness of MI-AEKF. In this paper, we use fitness function $f(k)$ to express the degree that estimation effect by MI-AEKF being approximate to the true value. There are many ways to define the fitness function. The most direct way is through the deviation between the estimated output voltage and experimental output voltage. Normally, the larger error of output voltage means the current multi-innovation length could not suitable for MI-AEKF. To validate the accuracy of the SOC estimation, the fitness function can be defined as follows:

$$f(k) = \left\| v_{term}(k) - \hat{v}_{term}(k) \right\|_2^2 \tag{34}$$

where $v_{term}(k)$ is the measured output voltage, and $\hat{v}_{term}(k)$ is the estimated output voltage.

For this research, the multi-innovation length L is selected from 1 to 10 with the step length 1. The assessment process is performed at each value of multi-innovation length, and the results are shown in Fig. 7. As can be seen from Fig. 7, the fitness function value typically changes when the value of the multi-innovation length L varies. It should be mentioned here that when the multi-innovation length are chosen from 5 to 10, the values of the fitness function are significantly beyond the range compared with other selected multi- innovation length. Hence, the range of length is chosen from 1 to 4. When the length is chosen as $L = 3$, the fitness function has the smallest value, which leads to the most accurate estimation of MI-AEKF. Therefore, the optimized length $L = 3$ is chosen for the estimation process by MI-AEKF to validate SOC estimation performance throughout this paper.

B. COMPARISON OF THE SOC ESTIMATION

1) ANALYSIS ON SOC ESTIMATION BY MI-AEKF

The simulation results by two algorithms under the DST and FUDS cycles are shown in Fig. 8. Of these, the estimation results of SOC is plotted in Fig. 8 (a and c). The reference SOC by CC method is formed by a black solid line, the red solid line represents the estimation results of SOC by AEKF and the blue solid line denotes the corresponding estimation results by MI-AEKF. According to the estimation results presented in Fig. 8 (a and c), the two algorithms based SOC estimation can both effectively track the SOC reference value. To make comparison more intuitive, the SOC estimation error by two algorithms under the DST and FUDS cycles are plotted in Fig. 8 (b and d). Among of them, it's obvious that the estimation error of SOC by the AEKF method with red

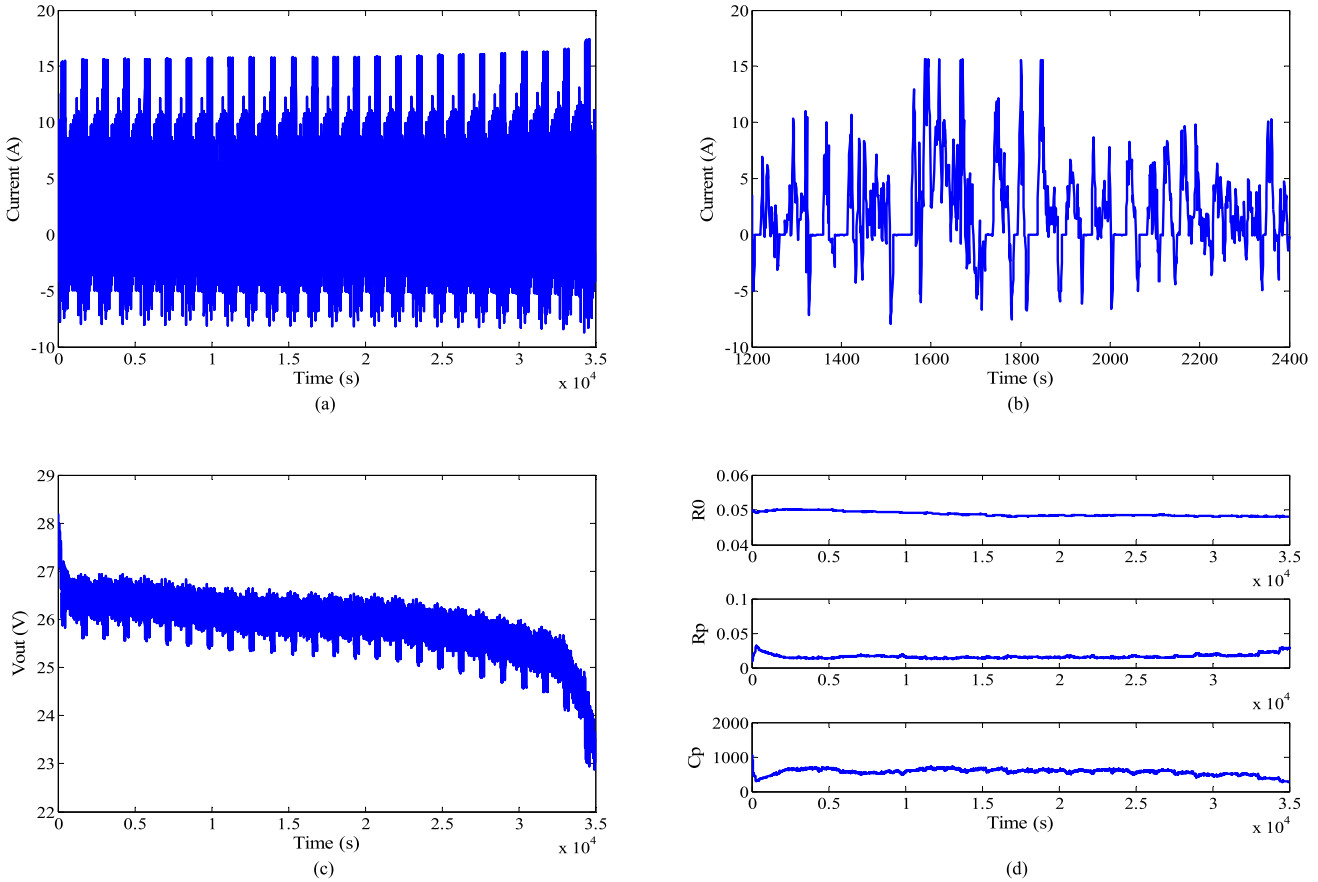

FIGURE 6. (a) Current under FUDS cycle; (b) enlarged current under FUDS cycle; (c) output voltage under FUDS cycle; (d) Identification value of R0, Rp, Cp under FUDS cycle.

TABLE 1. Comparison for the SOC estimation results without OCV compensation.

Methods	MI-AEKF(DST)	AEKF(DST)	MI-AEKF(FUDS)	AEKF(FUDS)
MAE (%)	1.2422	1.6862	1.5710	2.0093
AAE (%)	0.3353	0.7359	0.4695	0.8497

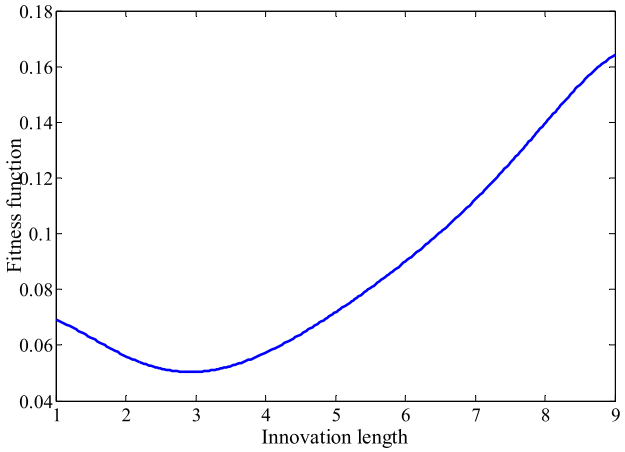

FIGURE 7. Fitness function of multi-innovation length.

solid line is larger than that of MI-AEKF method with blue solid line. It is observed that the maximum SOC error by AEKF is close to 2%, meanwhile the maximum SOC error by MI-AEKF is approximate to 1.6%. The MAE and AAE of AEKF and MI-AEKF are summarized in table 1. According to analysis above, the proposed MI-AEKF method has better performance for SOC estimation than AEKF method. Although the overall results of MI-AEKF and AEKF seem to be acceptable, there is scope for improvement. More specifically, the estimation error of two algorithm is relatively large when the SOC near to 20%.

2) ANALYSIS ON OCV COMPENSATION BASED SOC ESTIMATION

Since the local flat feature exists in the $OCV - SOC$ fitting curve, the OCV based SOC estimation is easily affected by OCV identification error in that special area. To further reduce the SOC estimation error in that local flat district, a novel OCV compensation strategy based on the output voltage deviation is incorporated into OCV calculation to assist MI-AEKF based SOC estimation. The simulation results by two algorithms with OCV compensation under the DST and

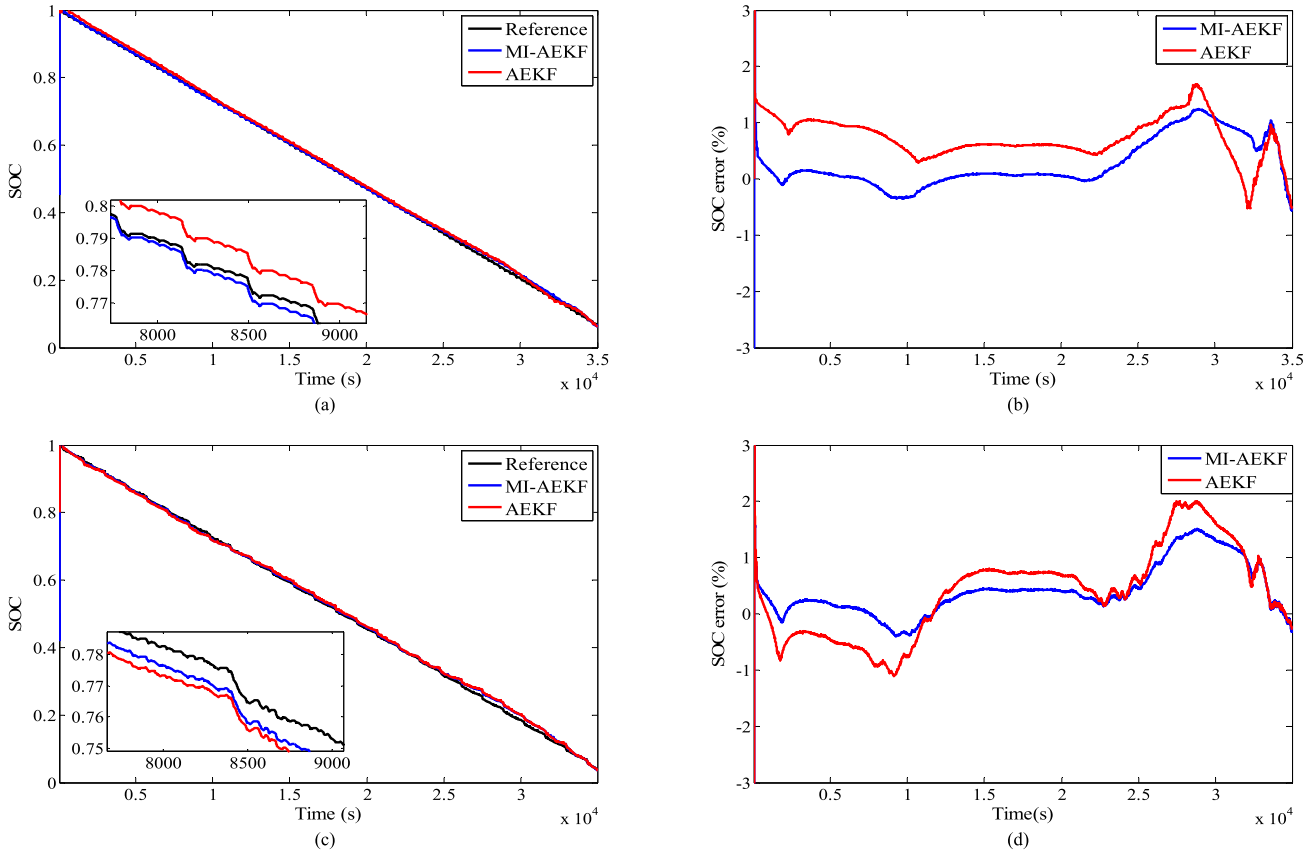

FIGURE 8. Comparison of SOC estimation under two cycles: (a) SOC estimation result under DST cycle; (b) SOC estimation errors under DST cycle; (c) SOC estimation result under FUDS cycle; (d) SOC estimation errors under FUDS cycle.

TABLE 2. Comparison for the SOC estimation results with OCV compensation.

Methods	MI-AEKF(DST)	AEKF(DST)	MI-AEKF(FUDS)	AEKF(FUDS)
MAE (%)	0.8721	1.2819	1.2853	1.8279
AAE (%)	0.2461	0.7278	0.3598	0.6973

FUDS cycles are shown in Fig. 9. Among them, the estimation result of SOC is plotted in Fig. 9 (a, c). The black solid line presents the reference SOC, the red dotted line denotes the estimation of SOC by AEKF, the red solid line represents the estimation of SOC by AEKF with OCV compensation, the blue dotted line shows the estimation of SOC by MI-AEKF and the blue solid line expresses the estimation of SOC by MI-AEKF with OCV compensation. According to the estimation results presented in Fig. 9 (a, c), the OCV compensation based strategy is good for effectively improving the tracking performance of SOC estimation.

Besides, the Fig. 9 (b, d) illustrates the SOC estimation error by the MI-AEKF with OCV compensation is minimal. That means the OCV compensation is beneficial to improve filtering effect of MI-AEKF and help for weakening effect of OCV identification error. Correspondingly, the SOC estimation error with red solid line is lower than that of red dotted line, that is, the OCV compensation also helps to reduce SOC estimation error by AEKF. It is observed that the maximum SOC error by AEKF is close to 1.8%, meanwhile the maximum SOC error by MI-AEKF is approximate to 1.3%. The MAE and AAE of AEKF and MI-AEKF are summarized in table 2. And, more remarkable, the SOC estimation error by MI-AEKF with OCV compensation is dramatically inhibited in those flat areas. Therefore, the combination of OCV compensation in MI-AEKF has evident advantage over AEKF for SOC estimation.

C. ANALYSIS ON INITIAL SOC ERRORS BASED SOC ESTIMATION

As the SOC estimation is presented in Section B, the precondition is that assumed initial value of SOC is reliable and equivalent to true initial value of SOC. However, due to the adverse impact of available capacity recovery or self-discharge effect, the initial errors of SOC may have a negative influence on the SOC estimation. To evaluate the possible negative influence by initial SOC errors, there are three levels of initialization errors on SOC: 10%, 20% and 30%

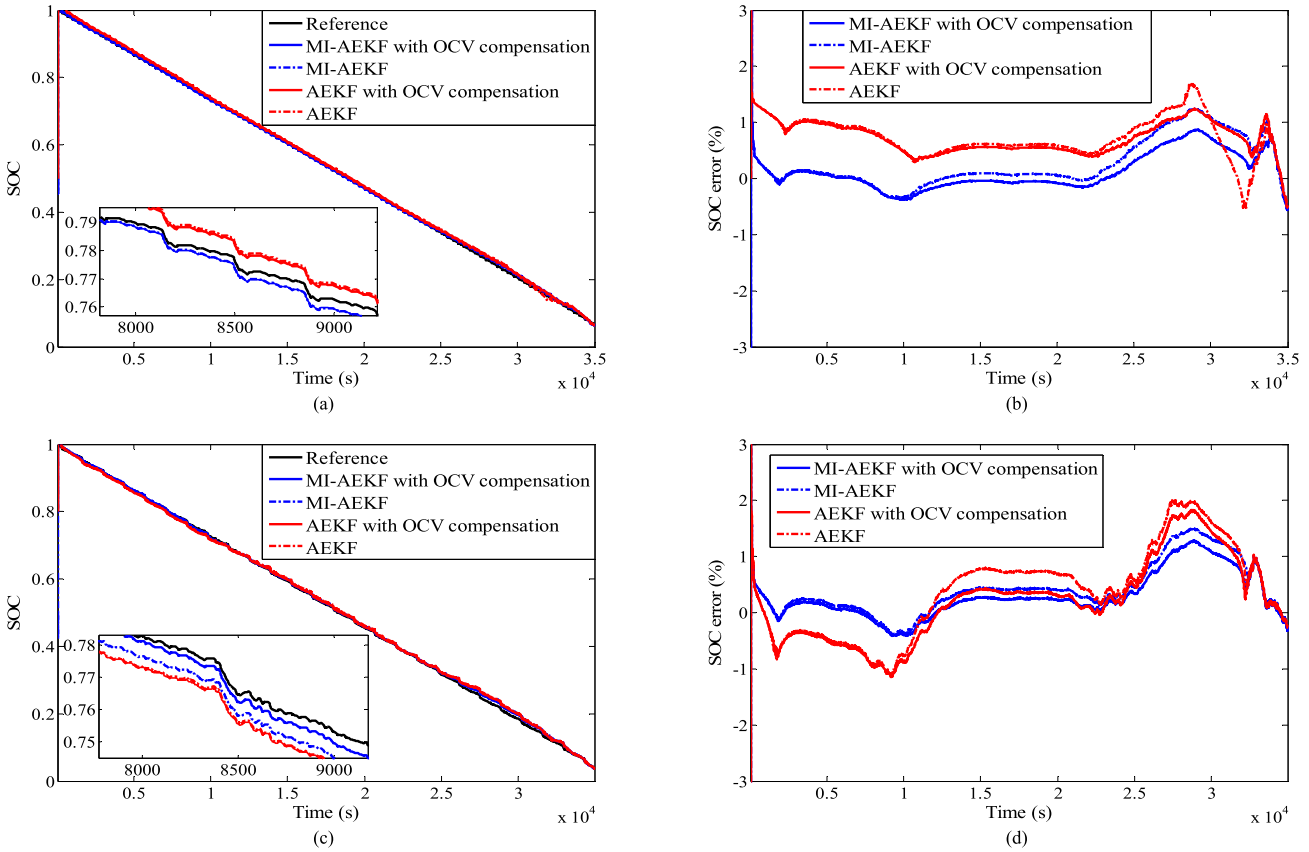

FIGURE 9. Comparison of SOC estimation with OCV compensation under two cycles: (a) SOC estimation result under DST cycle; (b) SOC estimation errors under DST cycle; (c) SOC estimation result under FUDS cycle; (d) SOC estimation errors under FUDS cycle.

TABLE 3. Comparison for the SOC estimation results with current noise.

Methods	MI-AEKF(DST)	AEKF(DST)	MI-AEKF(FUDS)	AEKF(FUDS)
MAE (%)	1.7153	2.3882	1.5008	1.9607
AAE (%)	0.4881	0.8767	0.5670	1.0680

respectively to apply for the OCV compensation based SOC estimator. The estimation results and errors of SOC are shown in Fig. 10, in which the black solid line presents the reference SOC, the blue solid line, red solid line and green solid line indicate the OCV compensation based SOC estimation with initial SOC errors of 10%, 20% and 30%, respectively, corresponding to initial SOC values of 90%, 80% and 70%, respectively. It is clear that the global SOC estimation errors with three levels of initialization errors are increased throughout the whole discharge process. However, the estimation errors are still within reasonable range, and the convergence and accuracy have not been markedly weakened. Although the differences of three estimation errors are relatively large at the beginning of discharging process, the three estimated SOC all can track to reference SOC rapidly and approximately in agreement with each other until the end of discharging.

D. ROBUSTNESS AGAINST NOISES

In the previous section of SOC estimation, the measurement is assumed as accurate data, which could be collected by power battery test system (Arbin EVTS). However, the actual measured value is not fully equivalent to true value in the process of practical operation, since the measured data is inevitably mixed with coupling noises, such as errors in sampling transducers. Therefore, it's necessary that BMS in EVs is capable of having strong robustness against coupling noises. To further assess the estimation effect of the MI-AEKF algorithm under measurement noise condition, a sequence of noise with characteristics of stochastic normal distribution is added to the measured current which can simulate actual current under two cycles. The mean value of the noise is zero and its standard deviation is 10^{-4}. The current with noise under DST cycle is shown

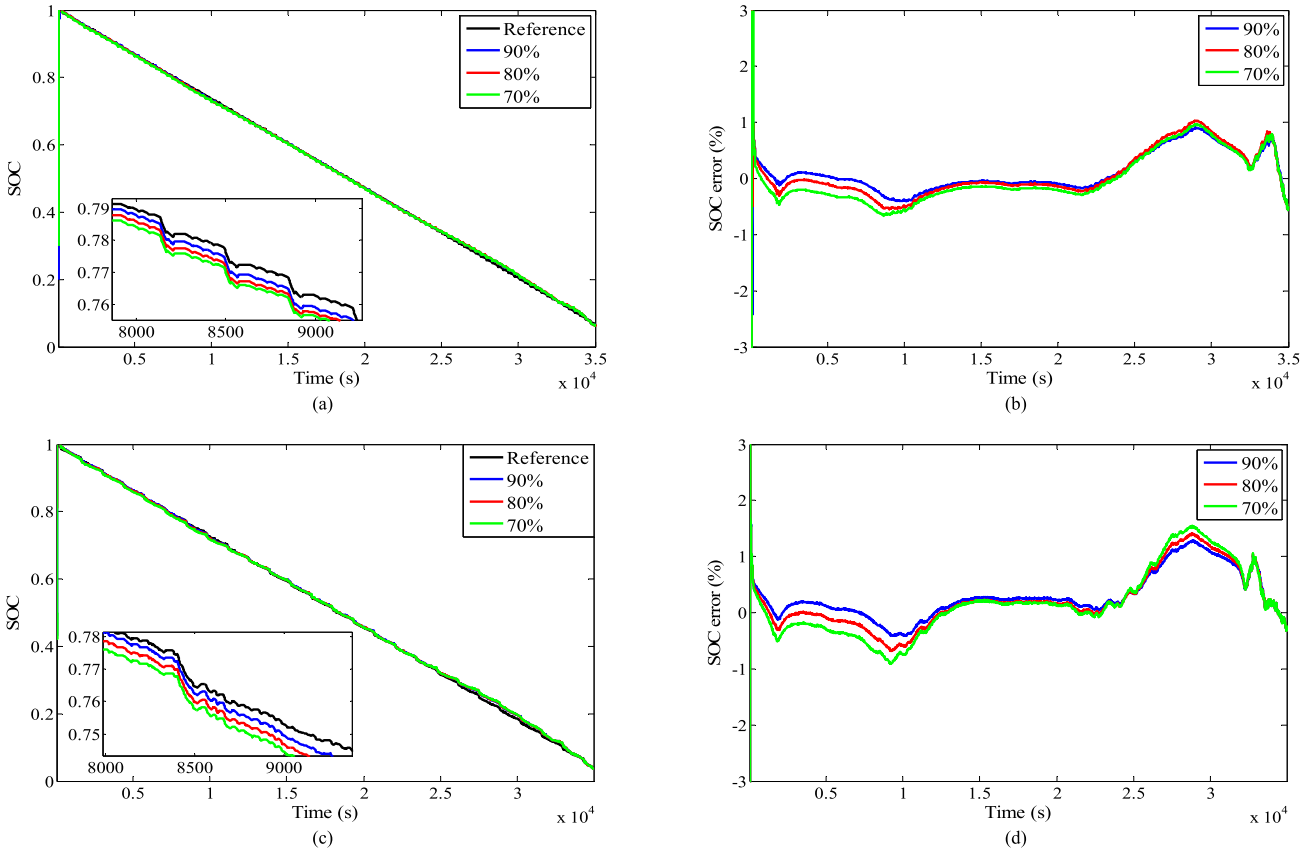

FIGURE 10. Comparison of SOC estimation with the initial SOC error under two cycle: (a) SOC estimation result under DST cycle; (b) SOC estimation errors under DST cycle; (c) SOC estimation result under FUDS cycle; (d) SOC estimation errors under FUDS cycle.

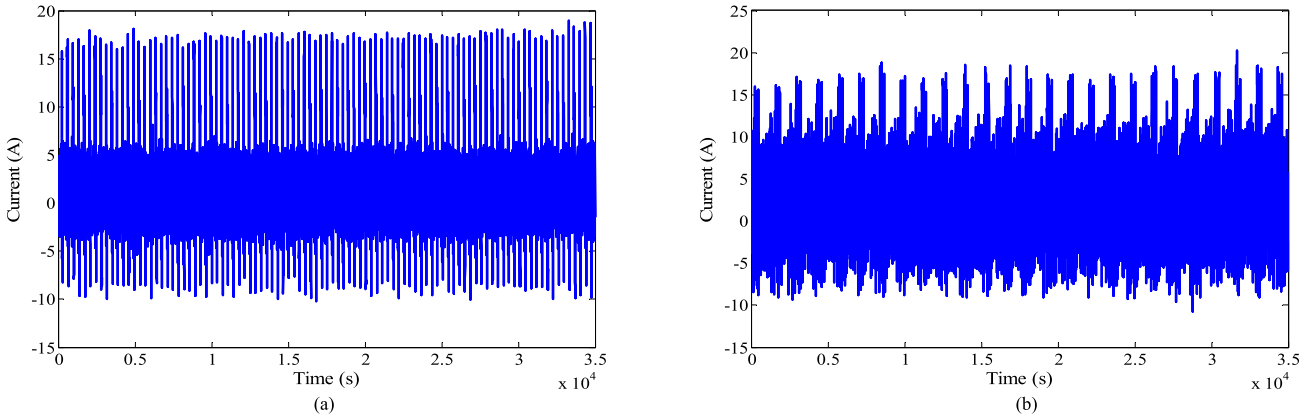

FIGURE 11. (a) Current with noise under DST cycle; (b) Current with noise under FUDS cycle.

in Fig. 11(a), the current with noise under FUDS cycle is shown in Fig. 11(b).

The SOC estimation results and errors influenced by current noise under two conditions are displayed in Fig. 12.

Among of them, the black line represents the reference SOC by CC method in Arbin EVTS. The red line denotes the estimation results and errors by AEKF with OCV compensation. The blue line represents the corresponding results and errors by MI-AEKF with OCV compensation. The MAE and AAE of SOC estimation by two methods are summarized in Table 3. As shown in Fig. 12 and Table 3, it is clear that SOC estimation errors of two algorithms based on OCV compensation fluctuate significantly due to the introduction of the current noise. The maximum SOC error by AEKF goes up over 2.3%, meanwhile the maximum SOC error by MI-AEKF increases over 1.7%. Although the MAE and AAE of two methods are both increased certain degree, the convergence speed and estimation performance of MI-AEKF is better than

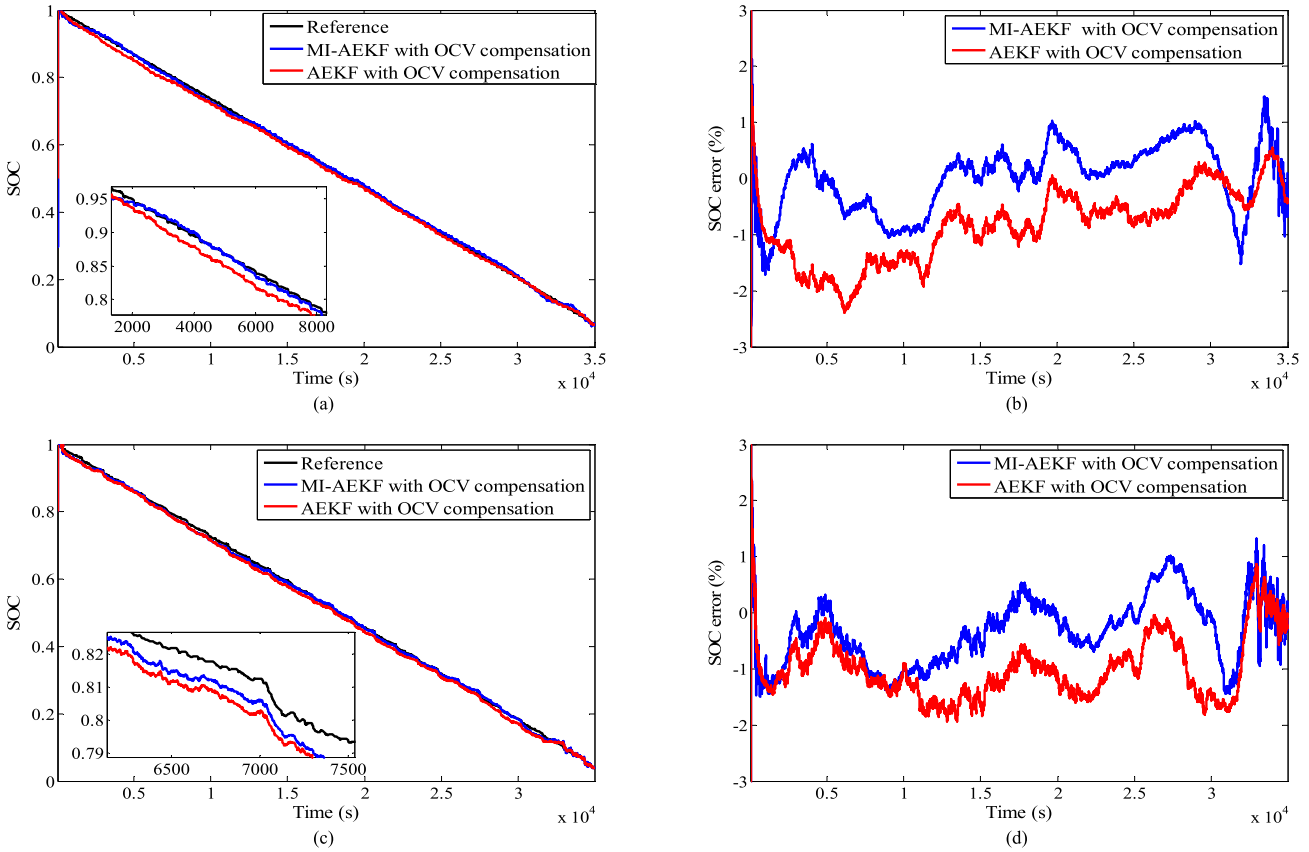

FIGURE 12. Comparison of SOC estimation against current noise under two cycle: (a) SOC estimation result under DST cycle; (b) SOC estimation errors under DST cycle; (c) SOC estimation result under FUDS cycle; (d) SOC estimation errors under FUDS cycle.

that of AEKF. The fast convergence and high precision also verify the robustness of the proposed MI-AEKF with OCV compensation method.

V. CONCLUSION

To achieve precise SOC estimation, a novel model- based SOC estimation method for LIB is proposed as the following items: (1) The one-order Thevenin ECM based on ARMA model analysis is utilized to represent external electrical specification of LIB and the VFFRLS-based method is applied to identify ECM parameters, which can weaken the impact of measurement with inevitable noises. (2) An improved AEKF approach is applied to develop an accurate and reliable SOC estimator based on the multi-innovation principle, and forgetting factors are added into each innovation to reduce cumulative influence of historical interference. (3) Because of the strong nonlinear characteristics in OCV-SOC fitting curve, especially the significant defect - the local flat effect in the curve induces extra errors of SOC estimation based on identified OCV. Therefore, an improved method for SOC estimation is designed based on the combination of MI-AEKF algorithm and feedforward compensation strategy. The MI-AEKF is used as SOC estimator for BMS. Meanwhile, the feedforward compensation is used to reform OCV prediction in real time. To evaluate the performance of the proposed algorithm, two working conditions are adopted to verify the SOC estimation, and added current noises to the working conditions are used to evaluate the robustness of the proposed method. Experimental results verified that presented methodology can obviously enhance the precision and anti-interference of SOC estimation for BMS.

APPENDIX

In this section, a convergence analysis based on MI-EKF is presented [37], [38].

In order to derive the convergence properties of the MI-AEKF algorithm, the following lemmas are required.

Lemma 1: Let a, x and y be non-negative real sequences satisfying

$$(x+y)^2 \le (1+a)\,x^2 + \left(1+\frac{1}{a}\right)y^2,\ a>0 \qquad (1)$$

Lemma 2: Assume that measurement noise γ_k is a stochastic noise with zero mean and variance σ^2: $E(\|\gamma_k\|^2) = \sigma^2$. And assume the gain vector $K(k)$ is persistently exciting, that is, there exist constants $0 < \alpha \le \beta < \infty$ and an integer $N \ge n$ such that the following persistent excitation condition holds:

$$\alpha I \le \frac{1}{N}\sum_{i=1}^{N} K(k-i+1)K^T(k-i+1) \le \beta I \qquad (2)$$

Define the estimation error: $\tilde{x}_k = \hat{x}_k - x_k$.

$$\begin{aligned}\tilde{x}_k &= \hat{x}_k - x_k \\ &= \hat{x}_{k|k-1} + K_{p,k}E_{p,k} - x_k \\ &= \hat{x}_{k|k-1} + K_{p,k}\left(Z_{p,k} - H_{p,k}\hat{x}_{k|k-1}\right) - x_k \\ &= \hat{x}_{k|k-1} - x_k + K_{p,k}\left(H_{p,k}x_k + V_{p,k} - H_{p,k}\hat{x}_{k|k-1}\right) \\ &= \hat{x}_{k|k-1} - x_k - K_{p,k}H_{p,k}\left(\hat{x}_{k|k-1} - x_k\right) + K_{p,k}V_{p,k} \\ &= \left[I - K_{p,k}H_{p,k}\right]\tilde{x}_{k|k-1} + K_{p,k}V_{p,k} \end{aligned} \tag{3}$$

By taking the 2-norm of both sides in the eq. (3) and using Lemma 1, it follows that:

$$\begin{aligned}\|\tilde{x}_k\|^2 &\le (1+a)\left\|\left[I - K_{p,k}H_{p,k}\right]\tilde{x}_{k|k-1}\right\|^2 \\ &\quad + \left(1+\frac{1}{a}\right)\left\|K_{p,k}V_{p,k}\right\|^2 \\ &\le (1+a)\left\|\left[I - K_{p,k}H_{p,k}\right]\right\|^2\left\|\tilde{x}_{k|k-1}\right\|^2 \\ &\quad + \left(1+\frac{1}{a}\right)\left\|K_{p,k}\right\|^2\left\|V_{p,k}\right\|^2 \\ &\le (1+a)\left\|\left[I - K_{p,k}H_{p,k}\right]\right\|^2\left\|\tilde{x}_{k|k-1}\right\|^2 \\ &\quad + \left(1+\frac{1}{a}\right)p\sigma^2\left\|K_{p,k}\right\|^2 \\ &\le (1+a)\left\|I + \left\|K_{p,k}\right\|^2\left\|H_{p,k}\right\|^2\right\|\left\|\tilde{x}_{k|k-1}\right\|^2 \\ &\quad + \left(1+\frac{1}{a}\right)p\sigma^2\left\|K_{p,k}\right\|^2 \\ &\le (1+a)\left\|\tilde{x}_{k|k-1}\right\|^2 \\ &\quad + (1+a)\left\|\tilde{x}_{k|k-1}\right\|^2\left\|K_{p,k}\right\|^2\left\|H_{p,k}\right\|^2 \\ &\quad + \left(1+\frac{1}{a}\right)p\sigma^2\left\|K_{p,k}\right\|^2 \end{aligned} \tag{4}$$

Taking the expectation of both sides in the eq. (4), we have:

$$\begin{aligned}E\|\tilde{x}_k\|^2 &\le E\left((1+a)\left\|\tilde{x}_{k|k-1}\right\|^2\right) \\ &\quad + E\left((1+a)\left\|\tilde{x}_{k|k-1}\right\|^2\left\|K_{p,k}\right\|^2\left\|H_{p,k}\right\|^2\right) \\ &\quad + E\left(\left(1+\frac{1}{a}\right)p\sigma^2\left\|K_{p,k}\right\|^2\right) \\ &\le (1+a)E\left(\left\|\tilde{x}_{k|k-1}\right\|^2\right) \\ &\quad + (1+a)E\left(\left\|\tilde{x}_{k|k-1}\right\|^2\left\|K_{p,k}\right\|^2\left\|H_{p,k}\right\|^2\right) \\ &\quad + \left(1+\frac{1}{a}\right)p\sigma^2E\left(\left\|K_{p,k}\right\|^2\right) \\ &\le (1+a)E\left(\left\|\tilde{x}_{k|k-1}\right\|^2\right) \\ &\quad + E\left(\left\|K_{p,k}\right\|^2\right)\left[\left(1+\frac{1}{a}\right)p\sigma^2 + (1+a)\right. \\ &\quad \left.\times E\left(\left\|\tilde{x}_{k|k-1}\right\|^2\left\|H_{p,k}\right\|^2\right)\right] \end{aligned} \tag{5}$$

Introducing the concept of greatest eigenvalue and assuming $\lambda_{\max}[x]$ represents the maximum eigenvalue of the gain vector $K_{p,k}$, we can get:

$$\begin{cases} E\left(\left\|K_{p,k}\right\|^2\right) \le E\left[\lambda_{\max}\left(K_{p,k}\cdot K_{p,k}^T\right)\right] \le p\beta_1 \\ E\left(\left\|H_{p,k}\right\|^2\right) \le E\left[\lambda_{\max}\left(H_{p,k}\cdot H_{p,k}^T\right)\right] \le p\beta_2 \end{cases} \tag{6}$$

Substituting Eq. (6) into Eq. (5), we can obtain Eq. (7) as follows.

$$\begin{aligned}E\left(\|\tilde{x}_k\|^2\right) &\le (1+a)E\left(\left\|\tilde{x}_{k|k-1}\right\|^2\right) \\ &\quad + p\beta_1(1+a)p\beta_2E\left(\left\|\tilde{x}_{k|k-1}\right\|^2\right) \\ &\quad + p\beta_1\left(1+\frac{1}{a}\right)p\sigma^2 \\ &\le \left[(1+a) + p\beta_1(1+a)p\beta_2\right]E\left(\left\|\tilde{x}_{k|k-1}\right\|^2\right) \\ &\quad + p\beta_1\left(1+\frac{1}{a}\right)p\sigma^2 \end{aligned} \tag{7}$$

Define

$$\begin{cases} (1+a) + p\beta_1(1+a)p\beta_2 = M \\ p\beta_1\left(1+\frac{1}{a}\right)p\sigma^2 = N \end{cases} \tag{8}$$

Then, we have

$$\begin{aligned}\lim_{k\to\infty}E\left(\|\tilde{x}_k\|^2\right) &\le \lim_{k\to\infty}ME\left(\left\|\tilde{x}_{k|k-1}\right\|^2\right) + N \\ &\le \lim_{k\to\infty}M^{k-1}E\left(\|\tilde{x}_1\|^2\right) + \frac{1-M^{k-1}}{1-M}N \end{aligned} \tag{9}$$

Based on the above analysis, the bounded convergence of $\tilde{x}_k$ based on MI-EKF is proved.

AUTHOR CONTRIBUTIONS

Xuanju Dang and Zheng Liu proposed original idea. Zheng Liu designed novel algorithm. Zheng Liu, Xuanju Dang and Benqin Jing performed and analyzed the experiments together. Zheng Liu wrote the original manuscript. Zheng Liu, Xuanju Dang and Benqin Jing revised the final manuscript.

CONFLICTS OF INTEREST

The authors declare no conflict of interest.

REFERENCES

[1] K. Liu, K. Li, and C. Zhang, "Constrained generalized predictive control of battery charging process based on a coupled thermoelectric model," *J. Power Sources*, vol. 347, pp. 145–158, Apr. 2017.

[2] X. Hu, H. Yuan, C. Zou, Z. Li, and L. Zhang, "Co-estimation of state of charge and state of health for lithium-ion batteries based on fractional-order calculus," *IEEE Trans. Veh. Technol.*, vol. 67, no. 11, pp. 10319–10329, Nov. 2018.

[3] J. Zhang, L. Zhang, F. Sun, and Z. Wang, "An overview on thermal safety issues of lithium-ion batteries for electric vehicle application," *IEEE Access*, vol. 6, pp. 23848–23863, May 2018.

[4] Z. P. Wang, C. H. Qu, L. Zhang, X. Xue, and J. Wu, "Optimal component sizing of a four-wheel independently-actuated electric vehicle with a real-time torque distribution strategy," *IEEE Access*, vol. 6, pp. 49523–49536, May 2018.
[5] M. M. Hoque, M. A. Hannan, A. Mohamed, and A. Ayob, "Battery charge equalization controller in electric vehicle applications: A review," *Renew. Sustain. Energy Rev.*, vol. 75, pp. 1363–1385, Aug. 2017.
[6] N. Takami, H. Inagaki, Y. Tatebayashi, H. Saruwatari, K. Honda, and S. Egusa, "High-power and long-life lithium-ion batteries using lithium titanium oxide anode for automotive and stationary power applications," *J. Power Sources*, vol. 244, pp. 469–475, Dec. 2013.
[7] T. Bruen and J. Marco, "Modelling and experimental evaluation of parallel connected lithium ion cells for an electric vehicle battery system," *J. Power Sources*, vol. 310, pp. 91–101, Apr. 2016.
[8] H. Shareef, M. M. Islam, and A. Mohamed, "A review of the stage-of-the-art charging technologies, placement methodologies, and impacts of electric vehicles," *Renew. Sustain. Energy Rev.*, vol. 64, pp. 403–420, Oct. 2016.
[9] Y. Xing, W. He, M. Pecht, and K. L. Tsui, "State of charge estimation of lithium-ion batteries using the open-circuit voltage at various ambient temperatures," *Appl. Energy*, vol. 113, pp. 106–115, Jan. 2014.
[10] N. Yang, X. Zhang, and G. Li, "State of charge estimation for pulse discharge of a $LiFePO_4$ battery by a revised Ah counting," *Electrochim. Acta*, vol. 151, pp. 63–71, Jan. 2015.
[11] X. Dang, L. Yan, H. Jiang, X. Wu, and H. Sun, "Open-circuit voltage-based state of charge estimation of lithium-ion power battery by combining controlled auto-regressive and moving average modeling with feedforward-feedback compensation method," *Int. J. Elect. Power Energy Syst.*, vol. 90, pp. 27–36, Sep. 2017.
[12] H. Sheng and J. Xiao, "Electric vehicle state of charge estimation: Nonlinear correlation and fuzzy support vector machine," *J. Power Sources*, vol. 281, pp. 131–137, May 2015.
[13] T. Hansen and C.-J. Wang, "Support vector based battery state of charge estimator," *J. Power Sources*, vol. 141, no. 2, pp. 351–358, Mar. 2005.
[14] J. Li, L. Wang, L. Chao, and M. Pecht, "State of charge estimation based on a simplified electrochemical model for a single $LiCoO_2$ battery and battery pack," *Energy*, vol. 133, pp. 572–583, Aug. 2017.
[15] C. Zhang, K. Li, L. Pei, and C. Zhu, "An integrated approach for real-time model-based state-of-charge estimation of lithium-ion batteries," *J. Power Sources*, vol. 283, pp. 24–36, Jun. 2015.
[16] X. Lai, Y. Zheng, and T. Sun, "A comparative study of different equivalent circuit models for estimating state-of-charge of lithium-ion batteries," *Electrochim. Acta*, vol. 259, pp. 566–577, Jan. 2018.
[17] B. Xia, Z. Sun, R. Zhang, D. Cui, Z. Lao, and W. Wang, "A comparative study of three improved algorithms based on particle filter algorithms in SoC estimation of lithium ion batteries," *Energies*, vol. 10, p. 1149, Aug. 2017.
[18] Z. Chen, Y. Fu, and C. C. Mi, "State of charge estimation of lithium-ion batteries in electric drive vehicles using extended Kalman filtering," *IEEE Trans. Veh. Technol.*, vol. 62, no. 3, pp. 1020–1030, Mar. 2013.
[19] Y. Li, C. Wang, and J. Gong, "A multi-model probability SOC fusion estimation approach using an improved adaptive unscented Kalman filter technique," *Energy*, vol. 141, pp. 1402–1415, Dec. 2017.
[20] L. Chen, L. Xu, and R. Wang, "State of charge estimation for lithium-ion battery by using dual square root cubature Kalman filter," *Math. Problems Eng.*, vol. 2017, Dec. 2017, Art. no. 5489356.
[21] Z. Zeng, J. Tian, D. Li, and Y. Tian, "An online state of charge estimation algorithm for lithium-ion batteries using an improved adaptive cubature Kalman filter," *Energies*, vol. 11, p. 59, Jan. 2018.
[22] Y. Xiang, X. J. Ma, C. Liu, R. S. Ke, and Z. X. Zhao, "Estimation of model parameters and SOC of lithium batteries based on IPSO-EKF," *Acta Armamentarii*, vol. 10, pp. 1659–1666, Oct. 2014.
[23] Y. Li, C. Wang, and J. Gong, "A combination Kalman filter approach for state of charge estimation of lithium-ion battery considering model uncertainty," *Energy*, vol. 109, pp. 933–946, Aug. 2016.
[24] R. Xiong, Q. Yu, L. Y. Wang, and C. Lin, "A novel method to obtain the open circuit voltage for the state of charge of lithium ion batteries in electric vehicles by using H infinity filter," *Appl. Energy*, vol. 207, pp. 346–353, May 2017.
[25] H. He, X. Zhang, R. Xiong, Y. Xu, and H. Guo, "Online model-based estimation of state-of-charge and open-circuit voltage of lithium-ion batteries in electric vehicles," *Energy*, vol. 39, no. 1, pp. 310–318, Mar. 2012.
[26] F. Feng, R. G. Lu, G. Wei, and C. B. Zhu, "Online estimation of model parameters and state of charge of $LiFePO_4$ batteries using a novel open-circuit voltage at various ambient temperatures," *Energies*, vol. 8, pp. 2950–2976, Apr. 2015.
[27] Z. B. Wei, J. Y. Zhao, D. X. Ji, and K. J. Tseng, "A multi-timescale estimator for battery state of charge and capacity dual estimation based on an online identified model," *Appl. Energy*, vol. 204, pp. 1264–1274, Oct. 2017.
[28] Q. Q. Yu, R. Xiong, C. Lin, W. X. Shen, and J. J. Deng, "Lithium-ion battery parameters and state-of-charge joint estimation based on H-infinity and unscented Kalman filters," *IEEE Trans. Veh. Technol.*, vol. 66, no. 10, pp. 8693–8701, Oct. 2017.
[29] H. Chaoui and S. Mandalapu, "Comparative study of online open circuit voltage estimation techniques for state of charge estimation of lithium-ion batteries," *Batteries*, vol. 12, pp. 1–13, Apr. 2017.
[30] J. Sabatier, J. M. Francisco, F. Guillemard, L. Lavigne, M. Moze, and M. Merveillaut, "Lithium-ion batteries modeling: A simple fractional differentiation based model and its associated parameters estimation method," *Signal Process.*, vol. 107, pp. 290–301, Feb. 2015.
[31] C. H. Weng, J. Sun, and H. Peng, "A unified open-circuit-voltage model of lithium-ion batteries for state-of-charge estimation and state-of-health monitoring," *J. Power Sources*, vol. 258, pp. 228–237, Jul. 2014.
[32] H. Pan, Z. Lü, W. Lin, J. Li, and L. Chen, "State of charge estimation of lithium-ion batteries using a grey extended Kalman filter and a novel open-circuit voltage model," *Energy*, vol. 138, pp. 764–775, Nov. 2017.
[33] C. Zhang, W. Allafi, Q. Dinh, P. Ascencio, and J. Marco, "Online estimation of battery equivalent circuit model parameters and state of charge using decoupled least squares technique," *Energy*, vol. 142, pp. 678–688, Jan. 2018.
[34] Y. Naderahmadian, M. Tinati, and S. Beheshti, "Generalized adaptive weighted recursive least squares dictionary learning," *Signal Process.*, vol. 118, pp. 89–96, Jan. 2016.
[35] M. Badoni, A. Singh, and B. Singh, "Variable forgetting factor recursive least square control algorithm for DSTATCOM," *IEEE Trans. Power Del.*, vol. 30, no. 5, pp. 2353–2361, Oct. 2016.
[36] M. Partovibakhsh and G. Liu, "An adaptive unscented Kalman filtering approach for online estimation of model parameters and state-of-charge of lithium-ion batteries for autonomous mobile robots," *IEEE Trans. Control Syst. Technol.*, vol. 23, no. 1, pp. 357–363, Jan. 2015.
[37] F. Ding, X. H. Wang, L. Ma, and L. Xu, "Joint state and multi-innovation parameter estimation for time-delay linear systems and its convergence based on the Kalman filtering," *Digit. Signal Process.*, vol. 62, pp. 211–223, Mar. 2017.
[38] S. Xie, D. Chen, X. Chu, and C. Liu, "Identification of ship response model based on improved multi-innovation extended Kalman filter," *J. Harbin Eng. Univ.*, vol. 39, no. 2, pp. 282–289, Feb. 2018.

ZHENG LIU received the M.Sc. degree in detection technology and automatic equipment from the Guilin University of technology, Guilin, China, in 2007, where he is currently pursuing the Ph.D. degree in instrument science and technology with the School of Electronic Engineering and Automation.

He is currently an Advanced Experimenter with the School of Electronic Information and Automation, Guilin University of Aerospace Technology. He has published more than ten papers and holds two patents. His research interests include nonlinear system filtering technology and the control theory of power battery energy management systems.

XUANJU DANG received the M.Sc. degree from the Shaanxi University of Science and Technology, Xian, China, in 1989, and the Ph.D. degree from Shanghai Jiao Tong University, Shanghai, China, in 2006.

He is currently a Professor with the School of Electronic Engineering and Automation, Guilin University of Electronic Technology. He has published more than 60 papers and holds 36 patents. His research interests include complex system modeling and control, neural networks modeling and design, and the control theory of electric vehicle battery management systems.

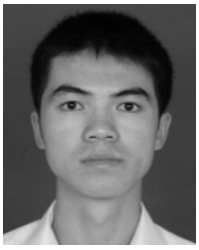

BENQIN JING received the M.Sc. degree in detection technology and automatic equipment from the University of Electronic Science and Technology of China, Chengdu, China, in 2010. He is currently pursuing the Ph.D. degree in instrument science and technology with the School of Electronic Engineering and Automation, Guilin University of Electronic Technology, Guilin, China.

He is currently a Lecturer with the School of Electronic Information and Automation, Guilin University of Aerospace Technology. He has published more than four papers and holds three patents. His research interests include embedded control technology and control of switched reluctance motor.